Electron–acoustic-phonon scattering rates in rectangular quantum wires

SeGi Yu* and K. W. Kim
Department of Electrical and Computer Engineering, North Carolina State University, Raleigh, North Carolina 27695-7911

Michael A. Stroscio and Gerald J. Iafrate
U.S. Army Research Office, P. O. Box 12211, Research Triangle Park, North Carolina 27709-2211

Arthur Ballato
Electronics and Power Sources Directorate, U.S. Army Research Laboratory, Ft. Monmouth, New Jersey 07703-5601
(Received 18 March 1994)

Electron–acoustic-phonon scattering in a rectangular quantum wire is studied. The Hamiltonian describing the deformation-potential interaction of confined acoustic phonons with carriers is derived by quantizing the appropriate, experimentally verified approximate compressional acoustic-phonon modes in a free-standing rectangular quantum wire. The scattering rate due to the deformation-potential interaction is obtained for GaAs quantum wires with a range of cross-sectional dimensions. The results demonstrate that a proper treatment of confined acoustic phonons may be essential to correctly model electron scattering rates at low energies in nanoscale structures.

I. INTRODUCTION

A number of proposed applications of mesoscopic electronic structures involve carrier transport at low temperatures and low carrier energies; frequently, the regime of interest is one where dimensional confinement modifies the phase space substantially. It is well known that in this low-temperature, low-energy regime,[1–6] acoustic phonons play an enhanced role in carrier scattering and may dominate over the scattering of carriers by optical phonons. In addition, in nanoscale structures it is possible that phase-space restrictions may weaken or forbid optical-phonon scattering processes that would normally dominate in bulk structures. Recently, there has been an extensive literature on the role of dimensional confinement in modifying longitudinal-optical (LO) phonon modes and their interactions with charge carriers in nanoscale and mesoscopic semiconductor structures (see, for example, Refs. 7–12 and the numerous papers referenced therein). On the other hand, there are relatively few treatments dealing with the role of dimensional confinement in modifying acoustic-phonon modes and their interactions with charge carriers.[2–4,13,14] In spite of the fact that there is an extensive literature on the theory of acoustic modes in conventional waveguides, resonators, and related structures, few efforts have been reported on formulating a theory of acoustic phonons in nanoscale structures, where both phonon confinement and a quantum-mechanical treatment of phonon normalization are essential. The necessity for such theoretical treatments has been demonstrated recently by experimental studies providing both direct and indirect[3,4] evidence of the importance of acoustic-phonon confinement in reduced dimensional electronic structures.

In this paper, we have obtained the normalized expressions for acoustic phonons confined in a free-standing rectangular quantum wire by appropriately quantizing the acoustic-phonon displacements. As is well known, there are no exact solutions for the complete set of phonon modes for a rectangular quantum wire; nevertheless, as for the case of LO phonon modes,[8] the approximate modes presented in this work provide simple and useful expressions, which are well suited for modeling the interaction of carriers with acoustic phonons. As a basis for investigating the role of reduced dimensionality on the coupling between acoustic phonons and carriers, we have formulated the interaction Hamiltonian for the deformation potential associated with confined acoustic-phonon modes in rectangular quantum wires. The resulting scattering rates (based on the golden rule approximation) are compared with those obtained from the bulk-phonon modes. For numerical calculations, GaAs is used as the material of choice throughout this study.

II. QUANTIZATION OF COMPRESSIONAL ACOUSTIC-PHONON MODES FOR A RECTANGULAR QUANTUM WIRE

The compressional, or dilatational, acoustic-phonon modes in free-standing rods of rectangular cross section have been examined both experimentally[15] and theoretically[16,17] by Morse in an extended study. Morse has derived an approximate set of hybrid compressional, or dilatational, acoustic-phonon modes,[16,17] which are found to accurately approximate the experimentally observed modes over a wide range of conditions.[15] Specifically, Morse has found that the approximate hybrid modes derived by assuming separable boundary conditions[16,17] have simple analytical representations and provide convenient approximations for the rectangular geometry when the cross-sectional dimensions have aspect ratios of approximately 2 or greater. For smaller aspect ratios (i.e., close to 1), Morse has argued correctly that it is necessary to turn to numerical solutions since exact

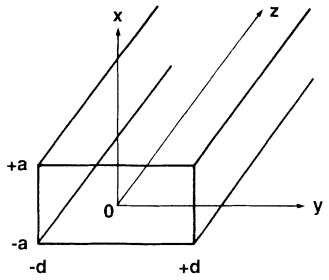

FIG. 1. Schematic drawing of a free-standing rectangular quantum wire considered in the analysis of electron–acoustic-phonon scattering.

analytical solutions for the compressional acoustic-phonon modes in a rectangular structure are not expressible analytically. In this paper, we shall restrict our analysis to rectangular quantum wires with aspect ratios of 2 or greater.

As depicted in Fig. 1, we consider a free-standing rectangular rod of infinite length in the z direction having an x-directed height (or thickness) $2a$, and a y-directed width $2d$; the origin of coordinates in the x-y plane is taken to be at the geometric center of the rectangular cross section, and the x-, y-, and z-directed acoustic-mode displacements are represented, respectively, by

$$u_1 = u(x,y)e^{i\gamma(z-ct)} , \tag{1}$$

$$v_1 = v(x,y)e^{i\gamma(z-ct)} , \tag{2}$$

$$w_1 = w(x,y)e^{i\gamma(z-ct)} , \tag{3}$$

where $\gamma = 2\pi/\lambda$, λ being the wavelength, γ is the z-directed free wave vector, and c is the phase velocity. Adopting Morse's form for the approximate separation-of-variables solution, the compressional waves for the "thickness" modes may be represented by

$$u = \{ A \sin k_1 x + B \sin k_2 x \} \cos(hy) , \tag{4}$$

$$v = \left\{ \frac{h}{k_1} A \cos k_1 x + C \cos k_2 x \right\} \sin(hy) , \tag{5}$$

$$w = i \left\{ -\frac{\gamma}{k_1} A \cos k_1 x + \frac{1}{\gamma}(k_2 B + hC) \cos k_2 x \right\} \cos(hy) , \tag{6}$$

where

$$k_1^2 + h^2 = \gamma^2[(c/c_d)^2 - 1] , \tag{7}$$

$$k_2^2 + h^2 = \gamma^2[(c/c_s)^2 - 1] , \tag{8}$$

and the compressional, or dilatational, sound speed c_d, as well as the transverse, or shear, sound speed c_s, are expressed in terms of the Lamé constants λ' and μ:

$$c_d^2 = (\lambda' + 2\mu)/\rho , \tag{9}$$

$$c_s^2 = \mu/\rho , \tag{10}$$

with ρ being the density of the medium. Substituting Eqs. (4)–(6) into the conditions that the T_{xx}, T_{yx}, and T_{zx} stress components vanish at $x = \pm a$, it follows that simultaneous equations for the amplitudes A, B, and C are given by

$$2Ah \sin k_1 a + Bh \sin k_2 a + Ck_2 \sin k_2 a = 0 , \tag{11}$$

$$-A(\gamma^2 + h^2 - k_2^2)\cos k_1 a + 2Bk_1 k_2 \cos k_2 a = 0 , \tag{12}$$

$$2A(h^2 + \gamma^2)\sin k_1 a + B(\gamma^2 + h^2 - k_2^2)\sin k_2 a = 0 . \tag{13}$$

When $k_2 \neq 0$, the condition that the determinant of coefficients vanishes requires that

$$\frac{\tan k_2 a}{\tan k_1 a} = -\frac{4k_1 k_2 (h^2 + \gamma^2)}{(h^2 + \gamma^2 - k_2^2)^2} , \tag{14}$$

which serves as the dispersion relation; this result is similar to the corresponding dispersion relation for the case of a slab.[18] Using Eq. (13) to solve for B in terms of A and applying the resultant expression in conjunction with Eq. (11) to solve for C in terms of A, Eqs. (3)–(6) may be written as

$$u_1 = A\{\sin k_1 x + \alpha \sin k_2 x\} \cos(hy) e^{i\gamma(z-ct)} , \tag{15}$$

$$v_1 = A \left\{ \frac{h}{k_1} \cos k_1 x + \beta \cos k_2 x \right\} \sin(hy) e^{i\gamma(z-ct)} , \tag{16}$$

$$w_1 = iA \left\{ -\frac{\gamma}{k_1} \cos k_1 x + \frac{1}{\gamma}(k_2 \alpha + h\beta) \cos k_2 x \right\} \times \cos(hy) e^{i\gamma(z-ct)} , \tag{17}$$

where α and β are defined by

$$B = -\frac{\sin k_1 a}{\sin k_2 a} \frac{2(h^2 + \gamma^2)}{(\gamma^2 + h^2 - k_2^2)} A = \alpha A , \tag{18}$$

and

$$C = -\left[\frac{k_2 h}{h^2 + \gamma^2} \right] B = \frac{\sin k_1 a}{\sin k_2 a} \frac{2k_2 h}{(\gamma^2 + h^2 - k_2^2)} A = \beta A . \tag{19}$$

Following the quantization procedure of Ref. 14, the normalization constant may be determined by quantizing the phonon modes so that,

$$\frac{1}{4ad} \int_{-a}^{+a} dx \int_{-d}^{+d} dy \{ uu^* + vv^* + ww^* \} = \frac{\hbar}{2M\omega_\gamma} , \tag{20}$$

where ω_γ is the radial frequency of the mode with wave vector γ. Performing the indicated integration, Eq. (20) yields the amplitude A in terms of the following equations:

$$\frac{A^2}{4ad}\left\{f_1(h,d)[f_2(k_1,a)+2\alpha g_1(k_1,k_2,a)+\alpha^2 f_2(k_2,a)]-f_1(h,d)\left[\frac{h^2}{k_1^2}f_1(k_1,a)+\frac{2\beta h}{k_1}g_2(k_1,k_2,a)+\beta^2 f_1(k_2,a)\right]\right.$$
$$+f_1(h,d)\left[\frac{\gamma^2}{k_1^2}f_1(k_1,a)-\frac{2}{k_1}(k_2\alpha+h\beta)g_2(k_1,k_2,a)+\frac{(k_2\alpha+h\beta)^2}{\gamma^2}f_1(k_2,a)\right]$$
$$\left.+2d\left[\frac{h^2}{k_1^2}f_1(k_1,a)+\frac{2\beta h}{k_1}g_2(k_1,k_2,a)+\beta^2 f_1(k_2,a)\right]\right\}=\frac{\hbar}{2M\omega_\gamma}\ , \quad (21)$$

where

$$f_1(h,d)=d\left[1+\frac{\sin(2hd)}{(2hd)}\right]\ , \quad (22)$$

$$f_2(h,d)=2d-f_1(h,d)\ , \quad (23)$$

$$g_1(k_1,k_2,a)=\frac{\sin(k_1-k_2)a}{(k_1-k_2)}-\frac{\sin(k_1+k_2)a}{(k_1+k_2)}\ , \quad (24)$$

$$g_2(k_1,k_2,a)=\frac{\sin(k_1-k_2)a}{(k_1-k_2)}+\frac{\sin(k_1+k_2)a}{(k_1+k_2)}\ . \quad (25)$$

Henceforth, A^2 is written as

$$A^2=\frac{2\hbar}{M\omega_\gamma B_\gamma}\ , \quad (26)$$

where B_γ is defined straightforwardly by Eqs. (21) and (26).

In accordance with the solutions of Morse,[16] the boundary conditions at $y=\pm d$ determine the value of h; however, the adjustment of h alone is sufficient to make T_{yy}, T_{xy}, and T_{zy} vanish at $y=\pm d$. For aspect ratios where the width of the rectangular cross section ($2d$) is greater than or approximately equal to twice the height ($2a$), this problem can be circumvented since the two shear stresses T_{xy} and T_{zy} become negligible. Accordingly, Morse chooses h so that the extensional stress T_{yy} vanishes; this condition requires

$$hd=(n+\tfrac{1}{2})\pi\ ,\quad n=0,1,2,\ldots\ . \quad (27)$$

The principal propagation mode (i.e., $n=0$ or $h=\pi/2d$) has no nodal surfaces parallel to the length. Motivated by the analysis in Sec. III, as well as by Morse's experimental observation that the principal mode is dominant,[15] the present paper considers the $n=0$ case for the thickness modes in numerical calculations. In addition to the thickness modes, another set of acoustic modes is observed experimentally.[15,16] These modes correspond to "width modes" and are determined in a manner similar to that used to determine the thickness modes. By satisfying the boundary conditions on the stress at $y=\pm d$, the solutions for the width modes show expressions analogous to Eqs. (15)–(17) with the roles of x and y as well as k and h interchanged, respectively. For these modes, k is then determined by approximate boundary conditions at $x=\pm a$.[16] The dispersion relation for the width mode is identical in form to Eq. (14), and the normalization procedure for proper quantization is as described in Eq. (20). As for the thickness modes, only the principal mode with $k=0$ is considered for the width modes.

We have calculated acoustic-phonon frequencies as a function of wave vector γ for the thickness and width modes in GaAs quantum wires. For this purpose, Eq. (14) may be written as

$$\frac{\tan(\pi\sqrt{\chi^2-\psi^2})}{\tan(\pi\sqrt{\epsilon\chi^2-\psi^2})}=-\frac{4\psi^2\sqrt{\chi^2-\psi^2}\sqrt{\epsilon\chi^2-\psi^2}}{(2\psi^2-\chi^2)^2}\ , \quad (28)$$

where

$$\chi^2=s^2(c/c_s)^2\ , \quad (29)$$

$$\psi^2=s^2+(ah/\pi)^2\ , \quad (30)$$

$$s=a\gamma/\pi\ , \quad (31)$$

$$\epsilon=(c_s/c_d)^2=(1-2\sigma)/2(1-\sigma)\ , \quad (32)$$

and σ is Poisson's ratio. Due to the periodic nature of trigonometric functions, the phonon frequency ω_γ ($=c\gamma$) has multiple solutions for a given γ and n (i.e., fixed h or k). Thus, an additional index m is needed to distinguish different modes. Figures 2 and 3 depict dispersion curves of the six lowest thickness modes ($h=\pi/2d$, $m=1,\ldots,6$) and the corresponding width modes ($k=0$, $m=1,\ldots,6$). The quantum wire cross-sectional dimensions are chosen to be 28.3×56.6 Å^2 for Fig. 2 and 50×200 Å^2 for Fig. 3, respectively. As expected, the width modes tend to have lower energies than the thick-

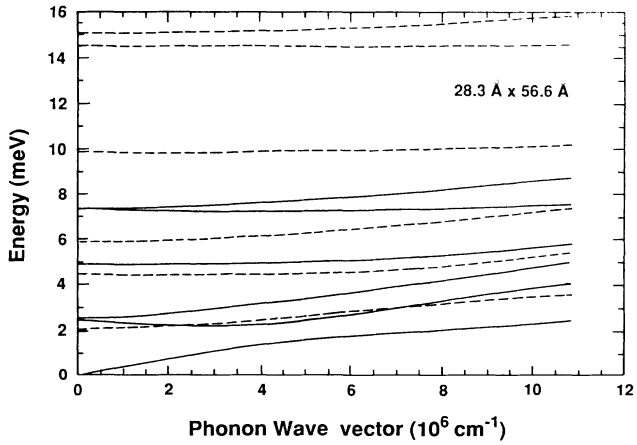

FIG. 2. Dispersion curves for the six lowest width and thickness modes ($m=1,\ldots,6$) of a 28.3×56.6-Å^2 GaAs quantum wire. The solid lines are for the width modes and the dashed lines are for the thickness modes.

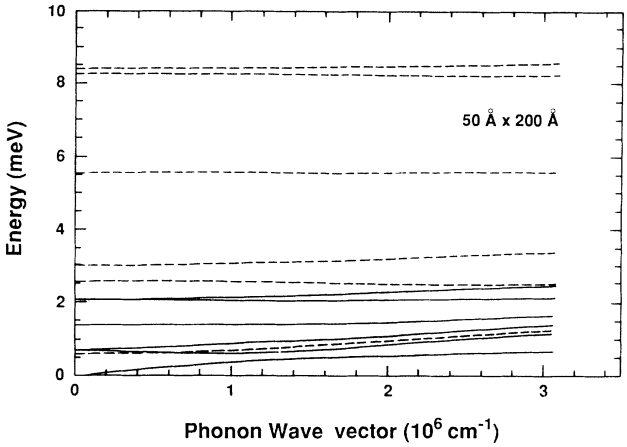

FIG. 3. Dispersion curves for the six lowest width and thickness modes ($m=1,\ldots,6$) of a 50×200-Å^2 GaAs quantum wire. The solid lines are for the width modes and the dashed lines are for the thickness modes.

ness modes, since the width is greater than the thickness for each of the cases represented in these figures.

III. ELECTRON–ACOUSTIC-PHONON SCATTERING RATES IN A RECTANGULAR QUANTUM WIRE

The deformation-potential interaction of the thickness mode is describable in terms of the Hamiltonian $H_{\rm def}$,

$$H_{\rm def}=E_a\nabla\cdot\mathbf{u}(\mathbf{r}) =E_a\sum_{\gamma,n,m}[c_{n,m}(\gamma)+c^{\dagger}_{n,m}(-\gamma)] \times\left[\frac{\partial u}{\partial x}+\frac{\partial v}{\partial y}+i\gamma w\right]e^{i\gamma z}, \tag{33}$$

where $c_{n,m}(\gamma)$ and $c^{\dagger}_{n,m}(-\gamma)$ are the usual annihilation and creation operators and

$$\mathbf{u}(\mathbf{r})=\sum_{\gamma,n,m}[c_{n,m}(\gamma)+c^{\dagger}_{n,m}(-\gamma)]\mathbf{u}(x,y,\gamma)e^{i\gamma z}. \tag{34}$$

The time-dependent factor $e^{-i\omega_\gamma t}$ is not included in Eqs. (33) and (34), since it will be included in the energy-conserving δ function in the golden rule. In Eqs. (33) and (34), the sum over γ represents the usual integration over wave vector, while the sums over n and m represent the addition of the various acoustic-phonon modes. For the normalized compressional, or dilatational, modes of Sec. II, it follows that

$$H_{\rm def}=\sum_{\gamma,n,m}E_a A\frac{\omega_\gamma^2}{c_d^2 k_1}\cos(k_1 x)\cos(hy) \times[c_{n,m}(\gamma)+c^{\dagger}_{n,m}(-\gamma)]e^{i\gamma z}, \tag{35}$$

where $\omega_\gamma^2=c^2\gamma^2$. Assuming the extreme quantum limit, the ground-state effective-mass electronic wave function is given by

$$\psi_q(x,y,z)=\frac{1}{\sqrt{ad}}\cos\left[\frac{\pi x}{2a}\right]\cos\left[\frac{\pi y}{2d}\right]e^{iqz}, \tag{36}$$

and the eigenenergy is

$$E=\frac{\hbar^2}{2m}\left[\left[\frac{\pi^2}{(2a)^2}+\frac{\pi^2}{(2d)^2}\right]+q^2\right]. \tag{37}$$

Hence, the matrix element $\langle q'|H_{\rm def}|q\rangle$ is given by

$$\langle q'|H_{\rm def}|q\rangle=\sum_{\gamma,n,m}E_a A\frac{\omega_\gamma^2}{c_d^2 k_1}\frac{\pi^2\sin k_1 a}{k_1 a(\pi^2-k_1^2a^2)} \times\frac{\delta_{q-q'+\gamma}}{\{(n+\frac{1}{2})\pi[1-(n+\frac{1}{2})^2]\}} \times[c_{n,m}(\gamma)+c^{\dagger}_{n,m}(-\gamma)]. \tag{38}$$

An examination of the n-dependent terms in Eq. (38) makes it apparent that they contribute to the matrix element squared in such a way that these terms for $n=1$ are only $\frac{1}{25}$ of their magnitude for $n=0$; a similar reduction occurs in going from $n=1$ to $n=2$ and it is clear that only the principal mode contributes significantly to Eq. (38), which was derived on the assumption that the carriers remain in the ground state of the extreme quantum limit, x-y potential.

Hence, the Fermi golden rule scattering rate corresponding to the matrix element of Eq. (38) is given by

$$\frac{1}{\tau}=\sum_{n,m}\int_{-\infty}^{+\infty}d\gamma\frac{L}{2\pi}\frac{2\pi}{\hbar}\left[E_a A_\gamma\frac{\omega_\gamma^2}{c_d^2 k_1}\right]^2 \times\left[\frac{\pi^2\sin k_1 a}{k_1 a(\pi^2-k_1^2a^2)}\right]^2\left[\frac{1}{(n+\frac{1}{2})\pi[1-(n+\frac{1}{2})^2]}\right]^2(N+\tfrac{1}{2}\pm\tfrac{1}{2})\delta\left[\frac{\hbar^2}{2m}(\gamma^2\mp 2q\gamma)\pm\hbar\omega_\gamma\right], \tag{39}$$

where A has been written as A_γ to indicate the γ dependence of A_γ, L is the normalization length along the axis of the quantum wire, and N is the usual temperature-dependent Bose-Einstein occupation number for the acoustic phonons. Introducing B_γ through Eq. (26) and defining factors Z_1 and Z_2, Eq. (39) may be written as

$$\frac{1}{\tau}=\sum_{n,m}\int_{-\infty}^{+\infty}d\gamma\,E_a^2\left[\frac{1}{2\rho abB_\gamma}\right]\frac{\omega_\gamma^3}{(c_d^2k_1)^2}Z_1^2Z_2^2(N+\tfrac{1}{2}\pm\tfrac{1}{2}) \times\delta\left[\frac{\hbar^2}{2m}(\gamma^2\mp 2q\gamma)\pm\hbar\omega_\gamma\right], \tag{40}$$

where

$$Z_1 = \frac{\pi \sin k_1 a}{k_1 a(\pi^2 - k_1^2 a^2)} \tag{41}$$

and

$$Z_2 = \frac{1}{(n+\frac{1}{2})\pi[1-(n+\frac{1}{2})^2]} \, . \tag{42}$$

The "width-mode" scattering rate may be readily formulated by following the procedure described above.

IV. NUMERICAL RESULTS

Deformation-potential scattering rates have been calculated in GaAs for two different quantum-wire aspect ratios. In the first case, the quantum-wire aspect ratio of width to height is taken as 2 and the dimensions of the rectangular cross section are taken as 28.3×56.6 Å^2 (i.e., 10×20 ML) and 100×200 Å^2. In the second case, the corresponding aspect ratio is taken as 4 and the wire dimensions are taken as 50×200 Å^2. In these calculations, an isotropic cubic medium has been assumed and the compressional, or longitudinal, sound speed has been taken to be that of GaAs; it should be noted that imposing both of these constraints makes it impossible to have a transverse sound speed matching that of GaAs. This is a consequence of the fact that GaAs may be treated as having an isotropic elastic tension only in a very rough approximation. In this paper, Poisson's ratio σ is taken to be $\frac{1}{3}$; this choice fixes the value of ϵ as given by Eq. (32).

Scattering rates for emission and absorption as functions of electron energy are plotted in Fig. 4 for a quantum wire with a 28.3×56.6 Å^2 cross section; these scattering rates are calculated at 77 K for both bulk acoustic modes and for the hybrid compressional modes. Figures 5 and 6 present results analogous to those of Fig. 4 but for different cross-sectional dimensions. Two distinct and important features are obvious from Figs. 4–6, which present related results for different dimensional parameters. First, the appearance of structure is prominent in the scattering rates (for confined phonons), which results from the energy threshold for the different mode values m of the thickness and width modes. As can be

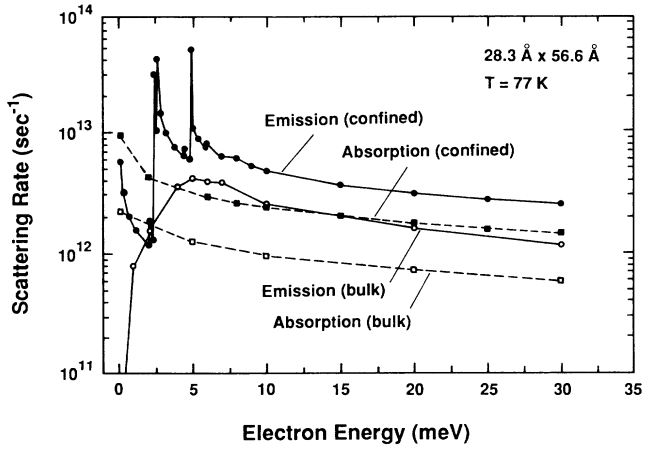

FIG. 4. Deformation-potential scattering rates for bulk and confined acoustic-phonon modes in a 28.3×56.6-Å^2 GaAs quantum wire at 77 K. Enhancements in the scattering rates for the case of confined acoustic modes occur at the onset of emission for the various width and thickness modes. These thresholds are at 0.03, 2.36, 2.55, 4.90, 7.30, and 7.40 meV for the width modes, and at 2.06, 4.44, 5.90, 9.87, 14.5, and 15.1 meV for the thickness modes. The plotting resolution depicted is not fine enough to illustrate fully the importance of the density-of-states effects in the rectangular quantum wire.

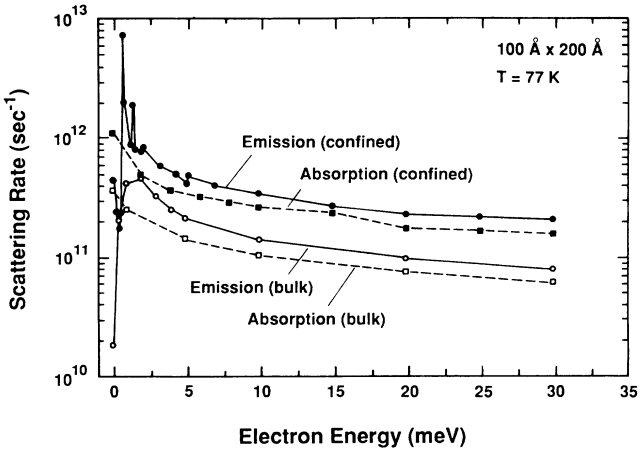

FIG. 5. Deformation-potential scattering rates for bulk and confined acoustic-phonon modes in a 100×200-Å^2 GaAs quantum wire at 77 K. Enhancements in the scattering rates for the case of confined acoustic modes occur at the onset of emission for the various width and thickness modes. These thresholds are at 0.03, 0.65, 0.75, 1.39, 2.06, and 2.12 meV for the width modes, and at 0.59, 1.26, 1.68, 2.80, 4.11, and 4.28 meV for the thickness modes. As in Fig. 4, the plotting resolution is limited.

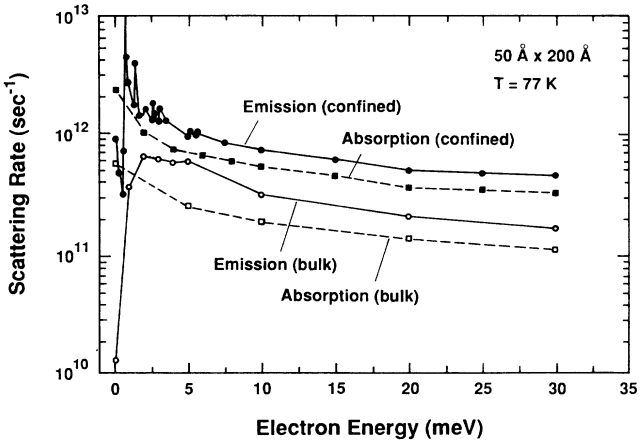

FIG. 6. Deformation-potential scattering rates for bulk and confined acoustic-phonon modes in a 50×200-Å^2 GaAs quantum wire at 77 K. Enhancements in the scattering rates for the case of confined acoustic modes occur at the onset of emission for the various width and thickness modes. These thresholds are at 0.03, 0.65, 0.75, 1.39, 2.06, and 2.12 meV for the width modes, and at 0.61, 2.58, 3.05, 5.56, 8.24, and 8.43 meV for the thickness modes. As in Figs. 4 and 5, the plotting resolution is limited.

seen from Figs. 4–6, each of these modes makes a notable contribution to the density of states and to the scattering rate. In particular, the scattering rates at low energies show pronounced peaks and are strongly enhanced due to the dominance of selected compressional modes in the emission process. Thus, it is essential to retain a number of acoustic modes for an accurate estimation of scattering rates. The results shown in Figs. 4–6 have been obtained by including the six lowest-order thickness modes as well as the six lowest-order width modes. Due to the limited resolution in plotting, the details of one-dimensional nature (such as the number of peaks and their heights) are not illustrated fully in these figures. The second important feature of Figs. 4–6 is that the scattering rates for the case of the hybrid compressional modes are higher than the corresponding bulk scattering rates. These enhanced scattering rates provided an indication that conceptual designs for mesoscopic devices need to be based on an awareness of the fact that confined acoustic modes may play a significant role in carrier transport in these devices. As shown in Fig. 5, for the case of a 100×200-Å^2 cross section we find similar scaling of the scattering rates with energy as for the case of Fig. 4; however, the rates are approximately an order of magnitude lower than those for the 28.3×56.6-Å^2 quantum wire of Fig. 4.

The hybrid modes considered in this paper contain both longitudinal and transverse components as is evident from Eqs. (15)–(18); as expected, only the longitudinal components contribute to the deformation potential of Eq. (35). The appearance of a hybrid-mode dispersion relation, Eq. (14), similar to that for the dilatational modes of a slab[18] is entirely reasonable, since the flexural modes are similar to the shear modes.[19] Such modes have strong transverse components and they make little contribution to electron–acoustic-phonon interaction through the deformation potential.

V. CONCLUSION

The results in this analysis suggest that it may be important to consider carrier–acoustic-phonon scattering processes when designing mesoscopic devices containing quantum-wire elements. Based on what appears to be the most complete set of approximate compressional modes available for a free-standing rectangular quantum wire,[16] it is demonstrated that the details of the modal structure need to be taken into account if deformation-potential scattering is to be modeled accurately. Further analysis is necessary to rigorously show that deformation-potential scattering rates by confined acoustic phonons exceed the corresponding rates obtained from bulk phonons in quantum wires; however, these results provide an indication that acoustic-phonon scattering may be enhanced considerably in some nanoscale structures.

ACKNOWLEDGMENTS

The authors would like to thank Dr. James W. Mink for his support and Professor M. N. Wybourne for advance information on his recent experimental evidence for acoustic-phonon confinement. The authors are also grateful to Professor V. Mitin, Dr. R. Mickevičius, and N. Bannov for many interactions on related confined-phonon effects in nanostructures. This work was supported, in part, by the Office of Naval Research and the U.S. Army Research Office.

*Also with Department of Physics, North Carolina State University, Raleigh, NC 27695.

[1]T. Kawamura and S. Das Sarma, Phys. Rev. B **45**, 3612 (1992).
[2]B. Hillebrands, S. Lee, G. I. Stegeman, H. Cheng, J. E. Potts, and F. Nizzoli, Phys. Rev. Lett. **60**, 832 (1988).
[3]J. Seyler and M. N. Wybourne, Phys. Rev. Lett. **69**, 1427 (1992); Z. V. Popvic, J. Spitzer, T. Ruf, M. Cardona, R. Notzel, and K. Ploog, Phys. Rev. B **48**, 1659 (1993).
[4]H. Benistry, C. M. Sotomayor-Torrés, and C. Weisbuch, Phys. Rev. B **44**, 10 945 (1991).
[5]B. A. Auld, *Acoustic Fields and Waves* (Wiley, New York, 1973).
[6]P. J. Price, Ann. Phys. (N.Y.) **133**, 217 (1981).
[7]N. Mori and T. Ando, Phys. Rev. B **40**, 6175 (1989).
[8]M. A. Stroscio, Phys. Rev. B **40**, 6428 (1989); K. W. Kim, M. A. Stroscio, A. Bhatt, V. V. Mitin, and R. Mickevičius, J. Appl. Phys. **70**, 319 (1991).
[9]K. W. Kim and M. A. Stroscio, J. Appl. Phys. **68**, 6289 (1990).
[10]R. Rücker, E. Molinari, and P. Lugli, Phys. Rev. B **45**, 6747 (1992).
[11]K. J. Nash, Phys. Rev. B **46**, 7723 (1992).
[12]M. A. Stroscio, G. J. Iafrate, K. W. Kim, M. A. Littlejohn, A. R. Bhatt, and M. Dutta, in *Integrated Optics and Optoelectronics,* edited by K.-K. Wong and M. Razeghi (SPIE, Bellingham, WA, 1993), Vol. CR45, p. 341.
[13]N. C. Constantinou, *Proceedings of NATO Advanced Research Workshop on Phonons in Nanostructures* (Kluwer, Boston, 1993), pp. 113–119.
[14]M. A. Stroscio and K. W. Kim, Phys. Rev. B **48**, 1936 (1993).
[15]R. W. Morse, J. Acoust. Soc. Am. **20**, 833 (1948).
[16]R. W. Morse, J. Acoust. Soc. Am. **22**, 219 (1950).
[17]R. W. Morse, Ph.D. thesis, Brown University, 1949.
[18]M. Redwood, *Mechanical Waveguides* (Pergamon, Oxford, 1960).
[19]R. A. Sykes, in *Quartz Crystals for Electrical Circuits,* edited by R. A. Heising (Van Nostrand, Toronto, 1946), p. 205.